

Revealing the Conformational Dynamics in a Single-Molecule Junction by Site- and Angle-Resolved Dynamic Probe Method

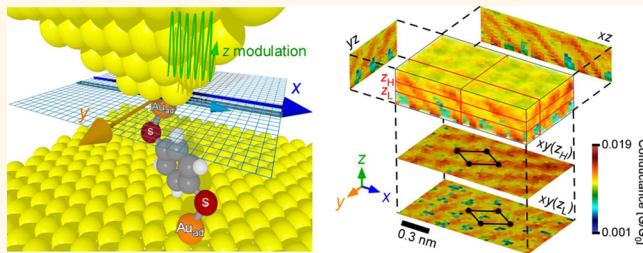
Shoji Yoshida, Atsushi Taninaka, Yoshihiro Sugita, Tomoki Katayama, Osamu Takeuchi, and Hidemi Shigekawa*

Faculty of Pure and Applied Sciences, University of Tsukuba, Tsukuba 305-8571, Japan

S Supporting Information

ABSTRACT: Single-molecule junctions have been extensively studied because of their high potential for future nanoscale device applications as well as their importance in basic studies for molecular science and technology. However, since the bonding sites at an electrode and the molecular tilt angles, for example, cannot be determined experimentally, analyses have been performed assuming the structures of such interactive key factors, with uncertainties and inconsistencies remaining in the proposed mechanisms. We have developed a methodology that enables the probing of conformational dynamics in single-molecule junctions simultaneously with the direct characterization of molecular bonding sites and tilt angles. This technique has revealed the elemental processes in single-molecule junctions, which have not been clarified using conventional methods. The mechanisms of the molecular dynamics in 1,4-benzenedithiol and 4,4'-bipyridine single-molecule junctions, which, for example, produce binary conductance switching of different types, were clearly discriminated and comprehensively explained.

KEYWORDS: molecular electronics, molecular junction, single molecule, scanning tunneling microscopy



Ideas involving the use of individual molecules as active electronic components to create new functional materials based on new concepts and/or combining them with, for example, semiconductor technologies to produce multifunctional devices have been among the central targets of researchers in recent decades. Single-molecule junctions have been a basic platform for experimental and theoretical studies.^{1–3} Mechanically controlled break junctions (MCBs) and scanning tunneling microscopy break junctions (STM-BJs) have generally been used to analyze the characteristics of single-molecule junctions.^{4,5} However, analyses have been performed assuming the interactive parameters of conformations such as bonding sites and molecular tilt angles, resulting in uncertainties and inconsistencies in the proposed mechanisms.^{6–9} Therefore, direct approach to experimentally visualize the conformational parameters is strongly required. Here, we present a methodology that enables the analysis of conformational dynamics in single-molecule junctions simultaneously with the direct and systematic characterization of molecular bonding sites, tilt angles, and deformation. The variations of the molecular dynamics in 1,4-benzenedithiol and 4,4'-bipyridine single-molecule junctions were clearly discriminated, and the mechanisms to produce binary conductance switching of different types were comprehensively explained.

RESULTS AND DISCUSSION

Three-Dimensional (3D) Dynamic Probe Measurement. Figure 1a schematically shows the 3D dynamic probe system.¹⁰ The current I flowing through a Au scanning tunneling microscopy (STM) tip/1,4-benzenedithiol (BDT)/Au substrate single-molecule junction was measured, while the STM tip, which was moved back and forth in the z -direction in accordance with a sinusoidal function (green line), was scanned two-dimensionally (x - and y -directions) (see Methods). Figure 1b shows an STM image of a Au(111) surface with six BDT molecules deposited on the elbow sites of a herringbone structure, as indicated by blue arrows, similarly to in a previous report,^{11,12} and its schematic conformation is shown in Figure 1c. The S atoms at both ends of the BDT molecule are terminated with a Au atom (adatom) labeled Au_{ad} .^{13,14} A Au/BDT/Au junction was formed by picking up one of the two Au_{ad} atoms with the STM tip after observing a target molecule (see Methods and Figure S1).^{10,15} Figures 1d and 1e show an example of the obtained data, in which the green, blue, and orange lines indicate the z modulation and x - and y -scans, respectively, and the red line

Received: September 16, 2016

Accepted: November 23, 2016

Published: December 2, 2016

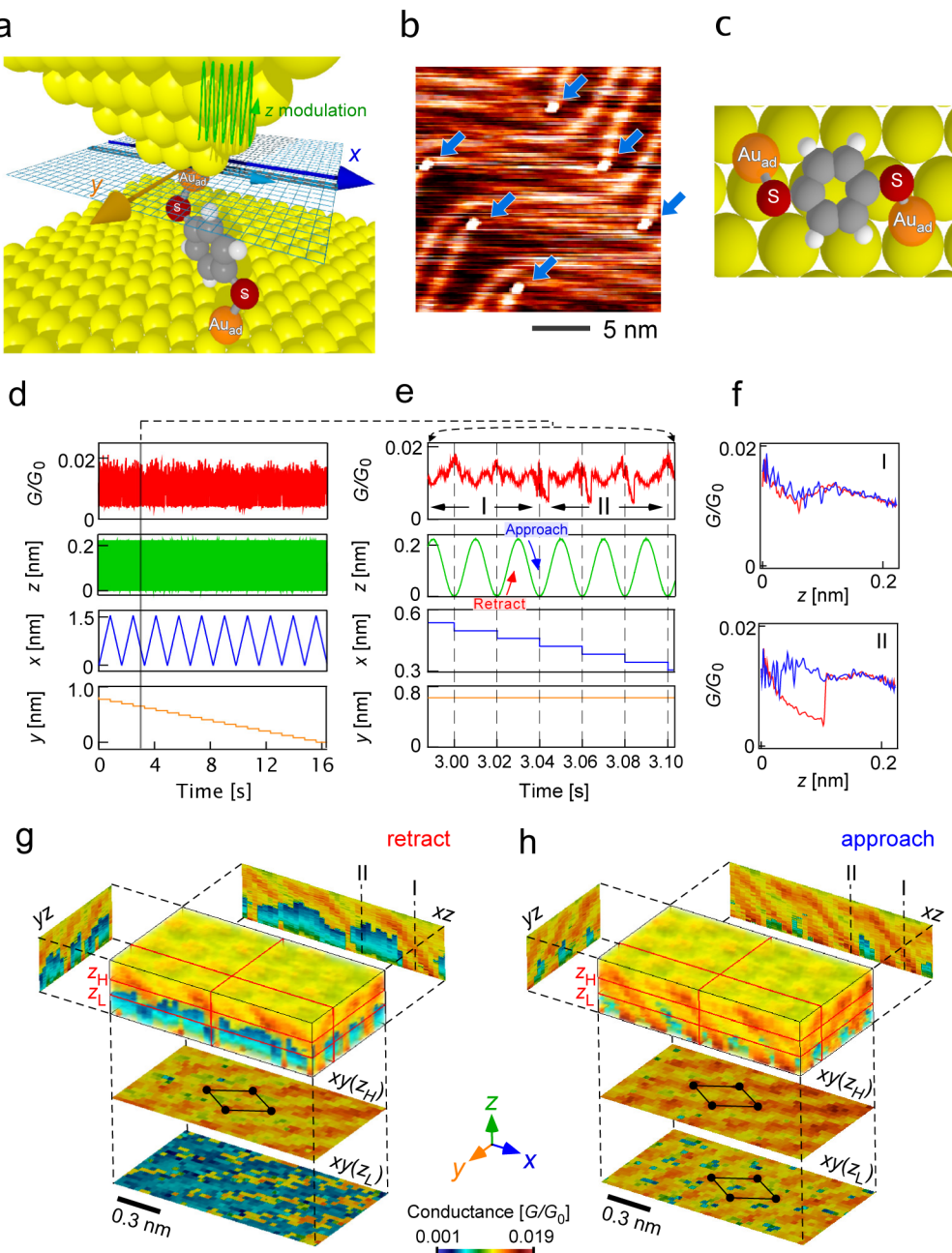


Figure 1. Measurement scheme and data display. (a) Schematic illustration of the 3D dynamic probe. (b) BDT molecules deposited on a Au(111) surface with the herringbone structure. (c) Schematic of the conformation of a BDT molecule on a Au(111) surface. (d, e) Measurement scheme and an example of a 3D dynamic probe signal. (f) Typical G–z curves obtained in regions I and II in (e). (g, h) 3D volume plots obtained while the STM tip was retracted and approached, respectively. The xy, yz, and xz cross sections, corresponding to the frames indicated by the red lines in the volume plots, are shown together. The Au(111) surface atomic structure is shown at the bottom.

shows the corresponding change in the normalized conductance G/G_0 ($G_0 = 2e^2/h$, where h is the Planck constant). Figure 1f shows typical $G-z$ curves obtained in regions I and II in Figure 1e. The red and blue $G-z$ curves were obtained, while the STM tip was retracted from and subsequently made to approach the Au surface, respectively. The $G-z$ curves show nonexponential characteristics, indicating the formation of a single-molecule junction (see Figure S1). As shown in Figure 1f, the red and blue $G-z$ curves have a similar form in region I but exhibit hysteresis in region II, showing the existence of binary switching of the conductance for the latter case. Figure 1g,h shows volume plots in the form of conductance maps as a function of the STM tip

apex (Au_{ad} atom) position (x, y, z) relative to its initial position ($0, 0, 0$) after the junction was formed (see Methods), which consist of the G/G_0 data obtained while the STM tip was retracted from and made to approach the Au surface, respectively. The cross sections of the xz-, yz-, and xy-planes, corresponding to the frames indicated by the red lines in the volume plots, are shown together. Two xy-planes at two different z (z_H and z_L) were found to show z -dependence. For $z = z_H$, the characteristic patterns in the brightness (map of G) in the xy-planes showed the periodicity of the Au(111) atomic structure for the cases of both retraction and approach, as indicated by the unit cell. Although the patterns obtained for STM tip retraction

and approach were similar for a large z ($z = z_H$), a difference between them appeared when z decreased. The conductance G decreased for the case of retraction, as indicated by a change in the color of the xy -plane into blue for a short z (z_L) with site dependence and as shown in Figure 1g. This produced the hysteresis observed in the $G-z$ curves in case II (Figure 1f), confirming the existence of site-dependent binary switching of the conductance with z -dependence. From the high reproducibility of the 3D patterns, the bond structure at the STM tip apex is considered to have been stable during the measurement (see Figure S2).

Determining Conformational Parameters from 3D Volume Plot. The complex variations in G shown in the volume plot in Figure 1g,h are considered to originate from the multiple factors determining the conformation in the junction, such as the molecular tilt angle,^{16–18} the site dependence^{19,20} (site hopping), and the deformation of the molecule;²¹ detailed information on these parameters is included in the volume plot. We analyzed the 3D volume plot to determine such parameters experimentally. Figure 2a,b, respectively, shows the z -dependences of the conductance patterns in Figure 1g,h in more detail. Three xy -planes at three different z (z_H , z_M , and z_L , corresponding to those marked in the xz cross sections) are shown. In Figure 2b, the pattern in the xy -plane is schematically drawn in the figure below the xy cross sections, which is superimposed on the Au(111) surface structure. When the bright positions, *i.e.*, high-conductance (H_C) regions, were superimposed on the hollow sites and on some of the bridge sites on the Au surface, excellent agreement was obtained. The pattern of the H_C regions shifted in the xy -plane with decreasing z , as indicated by the unit cells and arrows in Figure 2a,b, which produced the z -dependent trajectories of the bright arcs shown in the xz cross sections. As shown in the schematic illustrations of the junction in Figure 2c,d, the arcs drawn with the radius equal to the $Au_{ad}-Au_{ad}$ length (0.92 nm) with the hollow sites as the centers well reproduced the (H_C) pattern. Namely, when the Au_{ad} atom on the STM tip is at (x, y, z) in the H_C regions of the patterns while the STM tip is moved back and forth, the Au_{ad} atom on the other side is considered to be located on a hollow or a bridge site. The high reproducibility of the 3D patterns in the xy -planes that reflected the periodicity of the Au(111) atomic structure indicates that the substrate-side Au_{ad} atom reproducibly changed its position on the Au surface, while the STM tip position was three-dimensionally controlled. From the analysis of the 3D volume plot, we can obtain the conformational parameters. H^1 and H^2 and T in Figure 2c,d indicate the hollow and top sites of the Au surface, respectively. The purple and green curves labeled H^1 and H^2 were obtained by drawing arcs with radius equal to the $Au_{ad}-Au_{ad}$ length with the H^1 and H^2 sites as the centers, respectively. When the Au_{ad} at the STM tip was on arc H^2 , the Au_{ad} on the surface side was located at the H^2 site. While the STM tip was made to approach to arc H^1 , the Au_{ad} on the surface side is considered to have moved to the H^1 site. Figure 2e shows the parameters used to represent the molecular conformation in a junction. θ is the angle between the $Au_{ad}-Au_{ad}$ axis and the $\langle 121 \rangle$ axis in the xy -plane and φ is the tilt angle of the $Au_{ad}-Au_{ad}$ axis from the xy -plane. Here, the schematic was drawn with $\theta = 0^\circ$ for simplicity, and the actual positional relationships between the substrate and the STM tip (H^1 and H^2 positions), θ and φ were determined by 3D fitting of the arcs to the experimentally obtained H_C regions (see Figure S3 for more detail). Figure 2f shows the $G-z$ curves shown in Figure 1f with the obtained values of φ (the best fit for θ was 6° in this case). Conformational

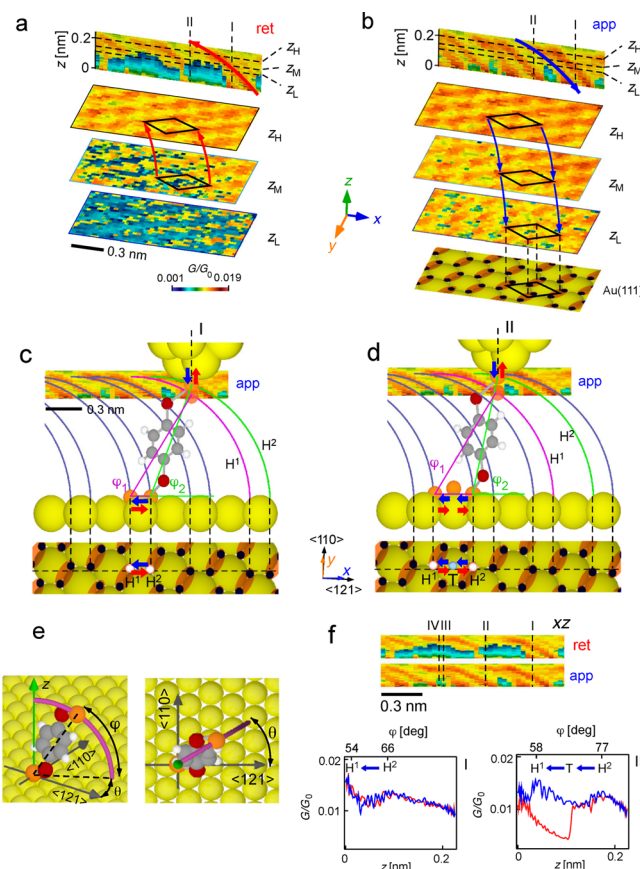


Figure 2. Models used to analyze the variation of G in the volume plots. (a, b) xz cross sections obtained from the volume plots shown in Figure 1g,h, respectively, and three H_C patterns in the xy cross sections obtained at three values of z_H , z_M , and z_L . (c, d) Schematic illustrations of the models used to analyze the variation of G in the volume plots. θ and φ are the angles of the $Au_{ad}-Au_{ad}$ axis from the $\langle 121 \rangle$ axis in the xy -plane and that from the xy -plane, respectively. Here, Au_{ad} atoms are schematically drawn as small circles, which may appear to shorten the distance between the STM tip and the Au substrate in the figures but does not affect the discussion in the text. T, H^1 , and H^2 indicate the top site and two hollow sites, respectively. The purple and green arcs labeled H^1 and H^2 have radii equal to the length of the $Au_{ad}-Au_{ad}$ axis with the H^1 and H^2 sites as the centers, respectively. (e) Schematic illustrations showing parameters θ and φ . (f) The xz cross sections corresponding to those in (a) and (b), and $G-z$ curves obtained for cases I and II shown in (c) and (d).

effects have generally been analyzed by comparing experimental results with simulations performed assuming the above parameters in various forms,^{6–9} with uncertainties and inconsistencies remaining in previously proposed models; these key factors can now be determined experimentally in the present method, which enables the discussion of conformational dynamics in single-molecule junctions simultaneously with the direct characterization of molecular bonding sites and tilt angles. For case I, when the STM tip is retracted, the Au_{ad} atom is considered to move from H^1 ($\varphi_1 = 54^\circ$) to H^2 ($\varphi_2 = 66^\circ$), as indicated by the blue arrows, which decreases G on the bridge site because the number of bonds is reduced. After the subsequent increase in G at the H^2 site, it decreases again with increasing z . For case II (Figures 2e and 3b), the Au_{ad} atom is considered to move from H^1 ($\varphi_1 = 58^\circ$) to H^2 (the other hollow site with $\varphi_2 = 77^\circ$) by passing through the T-site between them. A rapid decrease in G was observed when the Au_{ad} atom was on the T-

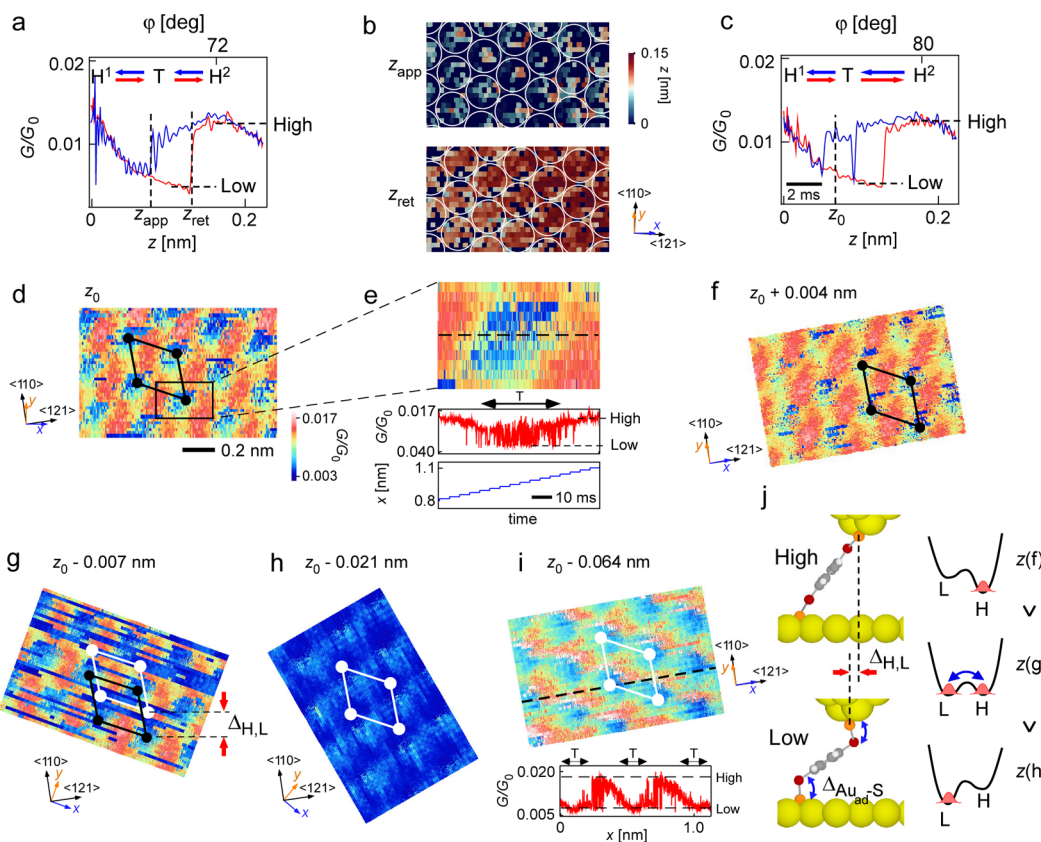


Figure 3. Fluctuation in the binary conformations. (a) $G-z$ curves obtained along line III in Figure 2a. (b) Mapping of z_{app} and z_{ret} determined in (a). (c) $G-z$ curves obtained along line IV in (a). Fluctuations were observed between the blue and red lines in case IV. (d) Conductance map obtained by xy -scan of the STM tip with the value of z kept at z_0 in (c). (e) Magnification of the rectangular area in (d) and cross sections along AB. The bottom graph shows the step-by-step changes in x . (f–i) The z dependence of H_C patterns obtained by xy -scan of the STM tip with respect to z_0 in (c) and (d) (see Figure S2 for $z_0 < z$). $\Delta H, L$ indicates the shift of the two unit cells. (j) Schematic illustration of a possible model for the binary switching between the high- (coplanar) and low-conductance (out of plane) states.

site. After the rapid increase in G at H^2 , it subsequently decreased again. When the STM tip was made to approach the Au surface after its retraction, the Au_{ad} atom moved along the same path as during the retraction in case I, while hysteresis was observed in case II, as shown in Figure 2f.

Analysis of the Binary Switching Producing the Hysteresis in the $G-z$ Curve. A $G-z$ curve with characteristics between those for cases I and II, *i.e.*, partial hysteresis, appeared at some STM tip positions, for example, along line III in Figure 2f, as shown in Figure 3a. Figure 3b shows the maps of z_{app} and z_{ret} defined in Figure 3a, indicating a change on the T-site and suggesting the existence of z - and/or site-dependent switching between binary conductance states with some activation barrier. In some cases (along line IV in Figure 2f), a fluctuation between the blue (approach) and red (retraction) lines was observed during the approach of the STM tip, as shown in Figure 3c. To observe this instability in more detail, we carried out an xy -scan of the STM tip with the value of z fixed at z_0 in Figure 3c (Figure 3d). As shown in the magnified image and the cross section (Figure 3e), the fluctuation occurred between binary states on the top site. Figure 3f–i shows the z - and scan angle dependences of the H_C patterns with respect to z_0 (see Figure S2 for $z_0 < z$). The area of preferentially staying at the low- G state increased with decreasing z independently of the scan angle and covered the entire surface in Figure 3h. Then G increased again in Figure 3i, in which fluctuation occurred at hollow sites. This change in G corresponds to the changes in the $G-z$ curves shown in Figure

3a,c. A positional shift of the two states, $\Delta_{H,L}$ is shown in Figure 3g. These results support the existence of conformation-dependent binary conductance states, which produce the hysteresis in the $G-z$ curve, in addition to a monotonic increase in G with decreasing $z(\varphi)$ ¹⁶ and a site-dependent change in G . Figure 3j shows a possible mechanism for the binary states, conformational change between coplanar (high) and out-of-plane (low) structures. The change is considered to be caused by z -dependent strain. The site dependence may be produced by the difference in the distance between the STM tip and Au surface, depending on the hollow site and top site. For the case of the $G-z$ curve without hysteresis (Figure 2f, case I), the molecular conformation remained in the high-conductance (coplanar) state independently of z in this region.

Theoretical Simulations of the Conformational Change. To understand the dynamics in more detail, we carried out simple simulations of cases I and II, while the STM tip was retracted as respectively shown in Figure 2c,d (see Methods). Figure 4a,b and Figure 4c,d show the $G-z$ curves and paths of the center of the Au_{ad} atom moved in accordance with the simulation for cases I and II, respectively. The obtained $G-z$ curves closely reproduced the experimental results. For case II, the conformational change is shown in Figure 4e, with the number of $\text{Au}_{\text{ad}}-\text{Au}$ bonds (Figure 4f) and the rotation angle of the benzene ring (Figure 4g) shown in Figure 4h. The following were observed: (1) H^1 to B: one of the three $\text{Au}_{\text{ad}}-\text{Au}$ bonds is broken and G decreases. (2) B to T: one of the two bonds is broken, and G

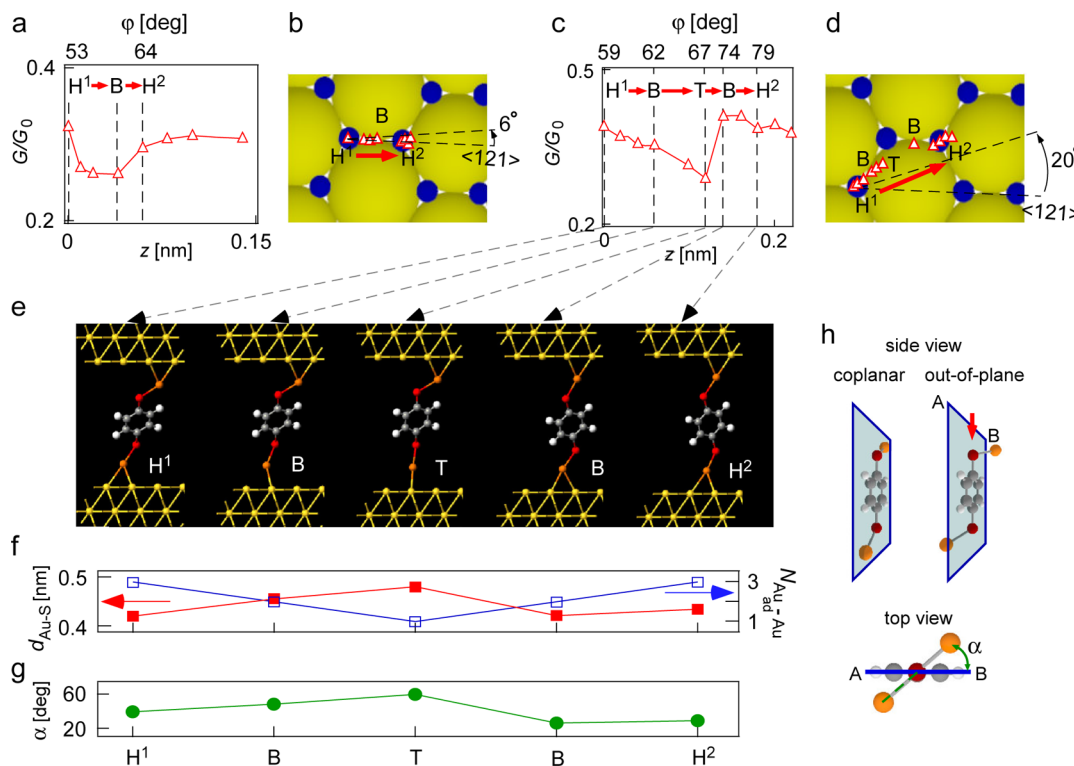


Figure 4. Conformational change and conductance characteristics in Au/BDT/Au junction obtained by simulation. (a, b) and (c, d) $G-z$ curves obtained by simulation and schematic illustrations showing the paths of the Au_{ad} atom (red open triangles), while the STM tip was retracted as shown in Figure 2c (for case I) and 2d (for case II), respectively. (e) Molecular conformations corresponding to the points shown in (c). (f, g) Number of Au_{ad}-Au bonds, the distance between the S and Au atoms, and the rotation angle α . (h) Coplanar and out-of-plane molecular conformations with the definition of α .

decreases to its lowest value. (3) T to B: G increases because the Au_{ad} atom forms a second bond (Figure 4f). In addition, the interaction between the S and Au atoms increases with decreasing distance between them owing to the rotation of the molecular plane (Figure 4g) from out-of-plane to coplanar configurations (Figure 4h) to reduce the conformation energy, which increases G . (4) B to H²: The formation of a third bond increases G , but the reduction in the interaction between the S and Au atoms, owing to the rotation of the molecular plane (benzene ring) between the coplanar and out-of-plane conformations, was found to play an important role in the change in conductance (see Figure S4 for more detail).

Analysis of $G-z$ Curve Over a Wide Range. We can now discuss the site and angle dependences separately. Figure 5a shows a volume plot obtained by measurement over a wide range ($z_{\text{p-p}} \sim 0.58$ nm). Figure 5b,c shows xz cross sections obtained from the volume plot in Figure 5a. We used the normalized $G_n (= (G(x, y, z) - G_{\text{avg}}(z))/G_{\text{sd}}(z))$ to obtain the G maps without the effect of the strong z -dependence, where $G_{\text{avg}}(z)$ and $G_{\text{sd}}(z)$ are the conductance averaged over each xy -plane and the standard deviation of G obtained for each of the xy -planes, respectively. Figure 5d shows $G-z$ curves obtained for motion over a wide range of z ($z_{\text{p-p}} \sim 0.58$ nm). Figure 5e,f shows magnifications of rectangular areas A and B in Figure 5d, respectively. The magnification of the rectangular area A in Figure 5e (region II) showing the change in G with z (*i.e.*, φ) is similar to those in Figures 1 and 3. The high reproducibility was obtained when stable 3D patterns were observed (see Figure S5 for the other case). As has been pointed out in a previous paper,^{16,22} the value of G/G_0 markedly increased to the orders of ~ 0.1 with

decreasing φ (region I in Figure 5d), while it decreased to 0.0005 with increasing z (Figure 5f, region III), which, for example, is caused by the change in the transmission pathway between the S atom and the surface Au atoms, as explained for the conformational change in Figure 4e. A possible model that explains the change in conductance in regions I, II, and III is illustrated in Figure 5g. (1) In region I ($\varphi < \sim 50^\circ$), the benzene ring is nearly parallel to the Au surface and the interaction between the π orbital and the surface Au increases, resulting in the formation of a channel between them with a high conductance exceeding $0.1G_0$.²² G decreases with increasing z owing to the reduction of the interaction. (2) In region II ($\sim 50^\circ < \varphi < 90^\circ$), the transmission between the S atom and the surface Au atoms changes, as explained for the conformational change in Figure 4e. (3) In region III ($\varphi \sim 90^\circ$), the distance between Au_{ad} and Au on the electrodes changes. The change in the low- G region shows a similar characteristic to that reported in a previous simulation.⁶ Despite a number of experimental and theoretical studies on this prototype single-molecule junction, a wide range of conductance of 0.001–0.1 G_0 order has been reported, and its relationship with conformational effects is not yet comprehensively understood.^{6–9,21–24} Here, we presented results obtained by a methodology of using a three-dimensional dynamic probe,¹⁰ and such effects were clearly visualized.

3D Dynamic Probe Analysis of 4,4'-Bipyridine Single-Molecule Junction. Finally, for comparison, we carried out site- and angle-resolved experiments on 4,4'-bipyridine (BPY), which has been considered to have angle-dependent binary conductance states for $\varphi < 90^\circ$,²⁵ and the results are shown in Figure 6. Figure 6a–d depicts a volume plot showing the value of G/G_0 and yz cross sections showing the values of G/G_0 and G_n ,

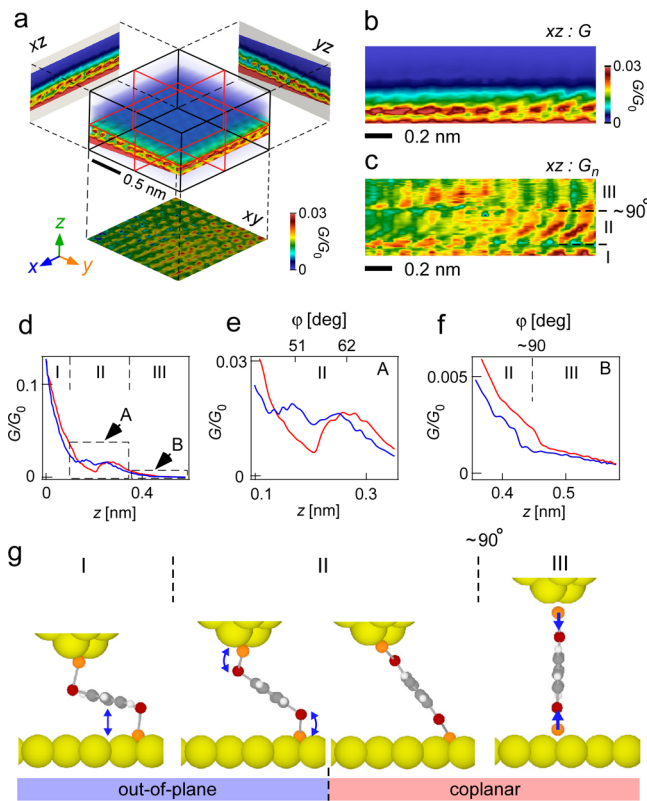


Figure 5. Angle-resolved analysis of conformational effect on conductance for Au/BDT/Au junction. (a) Volume plot. (b, c) The xz cross sections obtained from the volume plot shown in (a). We used the normalized $G_n (= (G(x, y, z) - G_{\text{avg}}(z))/G_{\text{sd}}(z))$ to show the G maps without the effect of the strong z dependence, where $G_{\text{avg}}(z)$ and $G_{\text{sd}}(z)$ are the conductance averaged over each xy-plane and the standard deviation of G obtained for each of the xy-planes. (d) G-z curves obtained for motion over a wide range of z ($z_{\text{p-p}} \sim 0.58$ nm). (e, f) Magnifications of rectangular areas A and B in (d), respectively. (g) Schematic illustrations to show the conformational change. A possible model that explains the change in conductance in regions I, II, and III is illustrated.

respectively. As shown in the G-z curve (Figure 6e), binary conductance states were clearly observed in regions I (High) and IV (Low). However, in contrast to the previous model,²⁵ they were observed for $\varphi < 90^\circ$ (region I) and after reaching $\varphi \sim 90^\circ$ (region IV) without angle dependence in both cases. Figure 6f-h shows the conductance maps obtained for regions II, III, and IV, respectively. The H_C pattern is similar to that obtained for BDT, and the conductance is higher at hollow and bridge sites than at top site.²⁶ As shown in Figure 6g, the image was fluctuated in region III, and a positional shift occurred, as schematically shown in Figure 6i, as a result of the shift between the two unit cells. A possible mechanism is shown in Figure 6j. In region I, the change in the molecular angle does not affect the N–Au angle, and the conductance is stable. After reaching $\varphi = 90^\circ$, a slow change in G occurs (region II), which is in good agreement with the result of calculation in ref 27 (Figure 4),^{26,27} i.e., the gradual decrease in the transmission caused by the change in the bond strength weekend by the increase in the N–Au distance. In region III, fluctuation in the molecular plane occurs because the steric hindrance between H (3,5- or 3',5'-) and surface Au atoms is reduced, resulting in the unstable conductance image shown in Figure 4f. After the conformational change has been completed, a low-transmission state continues until the bond is broken in

region IV. In contrast to the case of BDT, the change between the binary states occurs without activation barrier, that is, hysteresis does not appear. The positional shift in the H_C pattern is considered to be related to the change in the bonding conformation.

CONCLUSION

In conclusion, the dynamic probe technique that we have developed has revealed the elemental processes in single-molecule junctions, which have been hidden behind the multiple factors simultaneously measured in the conventional methods. The variations of the molecular dynamics in 1,4-benzenedithiol and 4,4'-bipyridine single-molecule junctions, which, for example, produce binary conductance switching of different types, were clearly discriminated, showing the high applicability of this method for the further development of molecular technologies.

METHODS

Sample and Tip Preparation. A clean flat Au(111) surface was prepared by evaporating Au to a thickness of about 100 nm on a mica substrate, which was subjected to Ar sputtering (5 min, $1 \mu\text{A}/\text{cm}^2$) and annealing (30 min, 700 K) for 3–5 cycles. Then the Au surface was exposed to 1,4-benzenethiol (BDT) molecules introduced through a variable leak valve (10 s, partial pressure: 1.0×10^{-6} Pa). The STM tip was formed by cutting a Au wire (0.3 mm diameter). All measurements were carried out in vacuum ($< 5.0 \times 10^{-8}$ Pa) at 83 K using a low-temperature STM (Omicron).

Measurement Scheme. After observing a target BDT molecule ($V_S = 0.2$ V, $I = +0.2$ nA), the feedback was turned off, and the sample bias voltage V_S was decreased to 10 mV because the bond was unstable at high bias voltages. Then, the STM tip was moved back and forth in the z-direction in accordance with a sinusoidal function ($z_{\text{p-p}} = 0.22$ nm, 50 Hz), and a two-dimensional scan was carried out for every cycle of z-modulation ($x, y, z: 41 \times 21 \times 200$ points in the case of Figure 1) over the molecule. Without the molecule, an exponential G-z curve was observed (Figure S1d), and an STM image of the molecule was obtained as shown in Figure S1e. To pick up one end of the molecule, the STM tip was manually made to approach the molecule while observing the change in G. When the molecule was picked up, a rapid increase in conductance was observed, and the G-z curve became nonexponential as shown in Figure 1f. Since the molecular junction was unstable above the herringbone structure, we moved the junction away from the structure for measurement. After observing a stable signal, we started measurement, with the coordinates of the first measurement set to (0, 0, 0). After cooling the STM unit with liquid nitrogen for over 1 week, the thermal drift over 30 min was reduced, which was sufficient time to obtain each 3D volume plot, for which 16 s was required. The effect of the sample gradient was removed by linear correction.

Simulation. We used Atomistic ToolKit software (version 12.8.2 Quantum Wise A/S), with density functional theory (DFT) within the local density approximation (LDA) using the Perdew–Zunger (PZ) exchange–correlation function²⁸ to simulate the optimized structures of the junction and the variation in its conductance while the STM tip was retracted. A double- ζ basis set was used for all atomic species, and the cutoff energy was set to 100 Ry. The sampling for Brillouin zone integration was performed at $3 \times 3 \times 400$ k-points. The conductance was calculated by the nonequilibrium Green's function (NEGF) method.^{29,30} A bias voltage of 10 mV was applied to the electrodes, assumed to comprise three layers of Au(111). Figure 4d shows snapshots of the conformational changes while the STM tip was retracted. In consideration of the adsorption sites of Au_{ad} at the STM tip, the initial values of θ were set to 6° and 20° for cases I and II to simplify the calculations, respectively. After the structure of the BDT molecule with the two Au_{ad} atoms on both sides was optimized, the distance between the two Au(111) electrodes was increased by 0.01–0.02 nm in each step. Structural optimization after each step was carried out for the

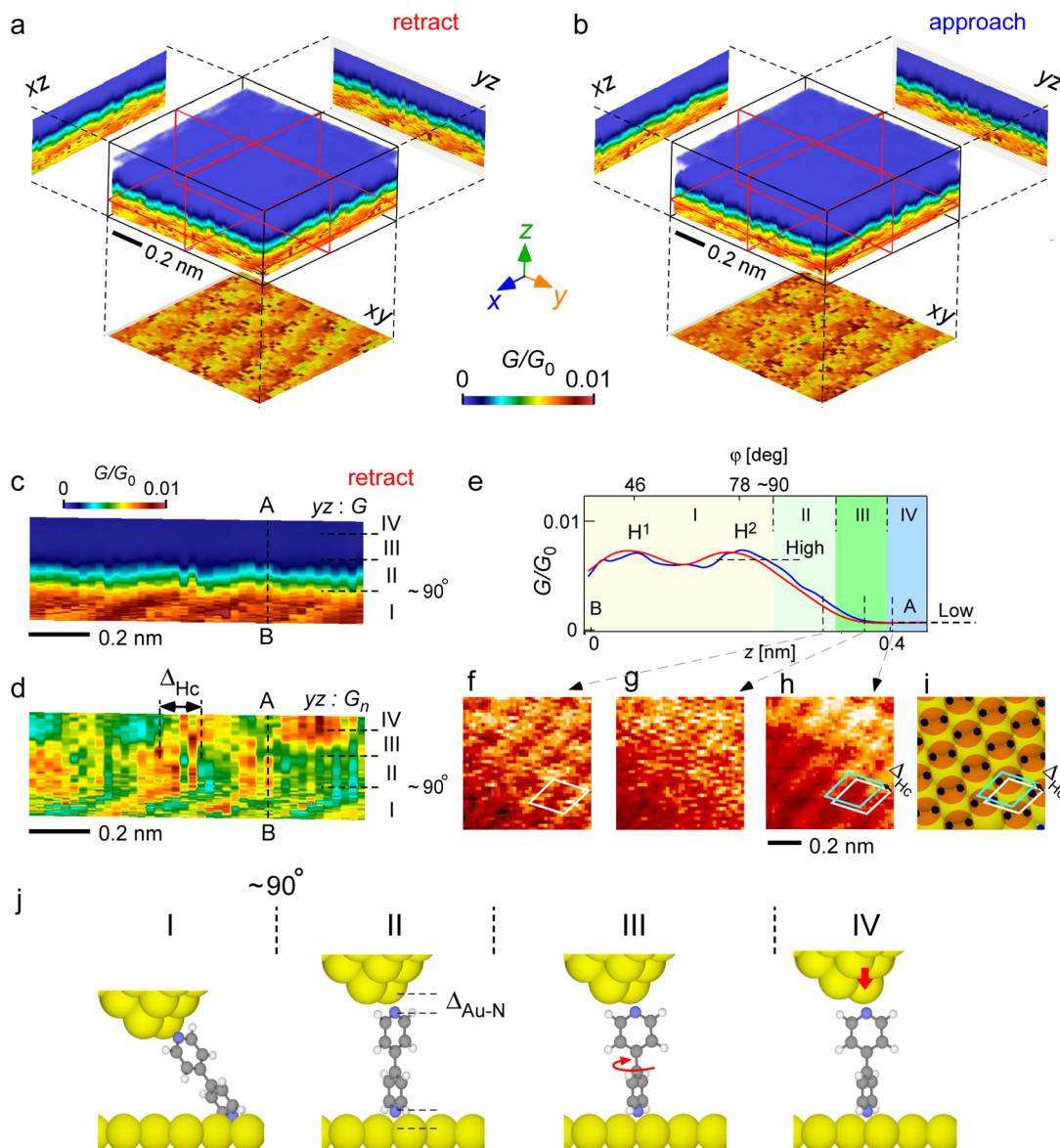


Figure 6. Angle-resolved analysis of conformational effect on conductance for Au/BPY/Au junction. (a, b) Volume plots obtained, while the STM tip was retracted and approached, respectively. (c, d) yz -cross sections obtained from the volume plot shown in a showing value of G/G_0 and G_n , respectively. (e) Typical $G-z$ curve. High and Low indicate the two binary conductance states. (f–h) The xy cross sections obtained at three different z points. White and light blue parallelograms indicate unit cells of the bright patterns in regions I and II, respectively. (i) Schematic of the bright pattern in region I with the two unit cells, showing their shift Δ_{HC} . (j) Schematic illustrations of a possible model for the conformational change in the regions I–IV corresponding to those in (e).

BDT molecule with the Au_{ad} atom (lower side) while fixing the structure of the upper-side Au_{ad} atom (STM tip side) in accordance with the experimental results (see Figure S2). Although DFT underestimates the energy gap,^{1,31} which may result in a larger conductance, the relative change in conductance is reliable.

ASSOCIATED CONTENT

S Supporting Information

The following files are available free of charge. The Supporting Information is available free of charge via the Internet at . three movies. The Supporting Information is available free of charge on the ACS Publications website at DOI: 10.1021/acsnano.6b06278.

Measurement scheme and example of data for BDT/ $Au(111)$, stability of the bond structure at the STM tip apex, variations in a volume plot and fitting, examination of

effect of bond structure at STM tip apex in the case of low G (PDF)

Movie 1: The y -dependence of G in the xz cross section (MPG)

Movie 2: The x -dependence of G in the yz cross section (MPG)

Movie 3: The z -dependence of G in the xy cross section (MPG)

AUTHOR INFORMATION

Corresponding Author

*E-mail: hidemi@ims.tsukuba.ac.jp.

ORCID

Hidemi Shigekawa: 0000-0001-9550-5148

Author Contributions

S.Y. worked in developing the 3D control system and data analysis. Y.S. performed the experiment with T.K., in which S.Y. instructed and assisted. A.T. considered the model simulations. O.T. provided technical advice. H.S. organized and supervised the project and edited the paper with S.Y.

Notes

The authors declare no competing financial interest.

ACKNOWLEDGMENTS

S.Y., A.T., O.T., and H.S. acknowledge the financial supports from Japan Society for the Promotion of Science Grant-in-Aid for Young Scientist (A) (16747650), for Challenging Exploratory Research (15K13269), and for Scientific Research (15H02023) and (15H05734), respectively.

REFERENCES

- (1) Cuevas, J. C.; Scheer, E. *Molecular Electronics: An Introduction to Theory and Experiment*; World Scientific: Hackensack, NJ, 2010.
- (2) Aradhya, S. V.; Venkataraman, L. Single-molecule junctions beyond electronic transport. *Nat. Nanotechnol.* **2013**, *8*, 399–410.
- (3) Ratner, M. A brief history of molecular electronics. *Nat. Nanotechnol.* **2013**, *8*, 378–381.
- (4) Xu, B.; Tao, N. J. Measurement of single-molecule resistance by repeated formation of molecular junctions. *Science* **2003**, *301*, 1221–1223.
- (5) Venkataraman, L.; Klare, J. E.; Tam, I. W.; Nuckolls, C.; Hybertsen, M. S.; Steigerwald, M. L. Single-molecule circuits with well-defined molecular conductance. *Nano Lett.* **2006**, *6*, 458–462.
- (6) Sergueev, N.; Tsetseris, L.; Varga, K.; Pantelides, S. Configuration and conductance evolution of benzene-dithiol molecular junctions under elongation. *Phys. Rev. B: Condens. Matter Mater. Phys.* **2010**, *82*, 073106.
- (7) French, W. R.; Iacovella, C. R.; Rungger, I.; Souza, A. M.; Sanvito, S.; Cummings, P. T. Structural Origins of Conductance Fluctuations in Gold-Thiolate Molecular Transport Junctions Structural Origins of Conductance Fluctuations in Gold-Thiolate Molecular Transport Junctions. *J. Phys. Chem. Lett.* **2013**, *4*, 887–891.
- (8) Strange, M.; Lopez-Acevedo, O.; Häkkinen, H. Oligomeric gold-thiolate units define the properties of the molecular junction between gold and benzene dithiols. *J. Phys. Chem. Lett.* **2010**, *1*, 1528–1532.
- (9) French, W. R. W.; Iacovella, C. R. C.; Cummings, P. P. T. Large-Scale Atomistic Simulations of Environmental Effects on the Formation and Properties of Molecular Junctions. *ACS Nano* **2012**, *6*, 2779–2789.
- (10) Nakamura, M.; Yoshida, S.; Katayama, T.; Taninaka, A.; Mera, Y.; Okada, S.; Takeuchi, O.; Shigekawa, H. Mechanically activated switching of Si-based single-molecule junction as imaged with three-dimensional dynamic probe. *Nat. Commun.* **2015**, *6*, 8465.
- (11) Yokoyama, T.; Yokoyama, S.; Kamikado, T.; Okuno, Y.; Mashiko, S. Selective assembly on a surface of supramolecular aggregates with controlled size and shape. *Nature* **2001**, *413*, 619–621.
- (12) Gao, L.; Liu, Q.; Zhang, Y. Y.; Jiang, N.; Zhang, H. G.; Cheng, Z. H.; Qiu, W. F.; Du, S. X.; Liu, Y. Q.; Hofer, W. A.; et al. Constructing an array of anchored single-molecule rotors on gold surfaces. *Phys. Rev. Lett.* **2008**, *101*, 197209.
- (13) Kestell, J.; Abuflaha, R.; Garvey, M.; Tysoe, W. T. Self-Assembled Oligomeric Structures from 1,4-Benzenedithiol on Au(111) and the Formation of Conductive Linkers between Gold Nanoparticles. *J. Phys. Chem. C* **2015**, *119*, 23042–23051.
- (14) Häkkinen, H. The gold-sulfur interface at the nanoscale. *Nat. Chem.* **2012**, *4*, 443–455.
- (15) Yasuda, S.; Yoshida, S.; Sasaki, J.; Okutsu, Y.; Nakamura, T.; Taninaka, A.; Takeuchi, O.; Shigekawa, H. Bond Fluctuation of S/Se Anchoring Observed in Single-Molecule Conductance Measurements using the Point Contact Method with Scanning Tunneling Microscopy. *J. Am. Chem. Soc.* **2006**, *128*, 7746–7747.
- (16) Haiss, W.; Wang, C.; Grace, I.; Batsanov, A. S.; Schiffrian, D. J.; Higgins, S. J.; Bryce, M. R.; Lambert, C. J.; Nichols, R. J. Precision control of single-molecule electrical junctions. *Nat. Mater.* **2006**, *5*, 995–1002.
- (17) Haiss, W.; Wang, C.; Jitchati, R.; Grace, I.; Martín, S.; Batsanov, A. S.; Higgins, S. J.; Bryce, M. R.; Lambert, C. J.; Jensen, P. S.; et al. Variable contact gap single-molecule conductance determination for a series of conjugated molecular bridges. *J. Phys.: Condens. Matter* **2008**, *20*, 374119.
- (18) Diez-Perez, I.; Hihath, J.; Hines, T.; Wang, Z.-S.; Zhou, G.; Müllen, K.; Tao, N. Controlling single-molecule conductance through lateral coupling of π orbitals. *Nat. Nanotechnol.* **2011**, *6*, 226–231.
- (19) Komoto, Y.; Fujii, S.; Nakamura, H.; Tada, T.; Nishino, T.; Kiguchi, M. Resolving metal-molecule interfaces at single-molecule junctions. *Sci. Rep.* **2016**, *6*, 26606.
- (20) Rascon-Ramos, H.; Artés, J. M.; Li, Y.; Hihath, J. Binding configurations and intramolecular strain in single-molecule devices. *Nat. Mater.* **2015**, *14*, 517–522.
- (21) Franco, I.; George, C. B.; Solomon, G. C.; Schatz, G. C.; Ratner, M. a. Mechanically activated molecular switch through single-molecule pulling. *J. Am. Chem. Soc.* **2011**, *133*, 2242–2249.
- (22) Kim, Y.; Pietsch, T.; Erbe, A.; Belzig, W.; Scheer, E. Benzenedithiol: A broad-range single-channel molecular conductor. *Nano Lett.* **2011**, *11*, 3734–3738.
- (23) Bruot, C.; Hihath, J.; Tao, N. Mechanically controlled molecular orbital alignment in single molecule junctions. *Nat. Nanotechnol.* **2011**, *7*, 35–40.
- (24) Ulrich, J.; Esrail, D.; Pontius, W.; Venkataraman, L.; Millar, D.; Doerr, L. H. Variability of conductance in molecular junctions. *J. Phys. Chem. B* **2006**, *110*, 2462–2466.
- (25) Quek, S. Y.; Kamenetska, M.; Steigerwald, M. L.; Choi, H. J.; Louie, S. G.; Hybertsen, M. S.; Neaton, J. B.; Venkataraman, L. Mechanically controlled binary conductance switching of a single-molecule junction. *Nat. Nanotechnol.* **2009**, *4*, 230–234.
- (26) Wu, X.; Li, Q.; Huang, J.; Yang, J. Nonequilibrium electronic transport of 4,4-bipyridine molecular junction. *J. Chem. Phys.* **2005**, *123*, 184712.
- (27) Hou, S.; Zhang, J.; Li, R.; Ning, J.; Han, R.; Shen, Z.; Zhao, X.; Xue, Z.; Wu, Q. First-principles calculation of the conductance of a single 4,4-bipyridine molecule. *Nanotechnology* **2005**, *16*, 239–244.
- (28) Perdew, J. P.; Zunger, A. Self-interaction correction to density-functional approximations for many-electron systems. *Phys. Rev. B: Condens. Matter Mater. Phys.* **1981**, *23*, 5048–5079.
- (29) Brandbyge, M.; Mozos, J.-L.; Ordejón, P.; Taylor, J.; Stokbro, K. Density-functional method for nonequilibrium electron transport. *Phys. Rev. B: Condens. Matter Mater. Phys.* **2002**, *65*, 165401.
- (30) Taylor, J.; Guo, H.; Wang, J. Ab initio modeling of quantum transport properties of molecular electronic devices. *Phys. Rev. B: Condens. Matter Mater. Phys.* **2001**, *63*, 245407.
- (31) Flores, F.; Ortega, J.; Vazquez, H. Modelling energy level alignment at organic interfaces and density functional theory. *Phys. Chem. Chem. Phys.* **2009**, *11*, 8658–8675.